ACS APPLIED MATERIALS & INTERFACES

Research Article

www.acsami.org

Hydroxylated Mesoporous Nanosilica Coated by Polyethylenimine Coupled with Gadolinium and Folic Acid: A Tumor-Targeted T_1 Magnetic Resonance Contrast Agent and Drug Delivery System

Guilong Zhang,[†,‡,§,⊥] Junlan Gao,[†,#] Junchao Qian,[‡] Lele Zhang,[#] Kang Zheng,[∥] Kai Zhong,[‡] Dongqing Cai,[§] Xin Zhang,*[,#] and Zhengyan Wu*[,§]

[§]Key Laboratory of Ion Beam Bioengineering, Hefei Institutes of Physical Science, Chinese Academy of Sciences and Anhui Province, Hefei, Anhui 230031, People's Republic of China

[⊥]University of Science and Technology of China, Hefei 230026, People's Republic of China

[#]School of Life Sciences, Anhui Agricultural University, Hefei 230036, People's Republic of China

[‡]High Magnetic Field Laboratory, Hefei Institutes of Physical Science, and [∥]Key Laboratory of Materials Physics, Institute of Solid State Physics, Chinese Academy of Sciences, Hefei 230031, People's Republic of China

Supporting Information

ABSTRACT: A pH-responsive nanoplatform, hydroxylated mesoporous nanosilica (HMNS) coated by polyethylenimine (PEI) coupled with gadolinium and folic acid (FA) (Gd-FA-Si), was designed to deliver anticancer drug targeting and to promote contrast effect for tumor cells using magnetic resonance (MR) spectrometer. Doxorubicin (DOX) was chosen as the anticancer drug and loaded into nanopores of HMNS, then its release in simulated body fluid could be controlled through adjusting the pH. This nanoplatform could significantly enhance the MR contrast effect, and the highest theoretical relaxivity per nanoplatform could even be approximately 1.28×10^6 $mm^{-1}s^{-1}$ because of the high Gd payload (2.61×10^5 per nanoplatform). The entire system possessed a high targeting performance to Hela and MDA-MB-231 cells because the FA located in the system could specifically bind to the folate−receptor sites on the surface of cell. Compared with free DOX, the nanoplatform presented a higher cell inhibition effect on the basis of cell assay. Therefore, this nanoplatform could be potentially applied as a tumor-targeted T_1 MR contrast agent and pH-sensitive drug carrier system.

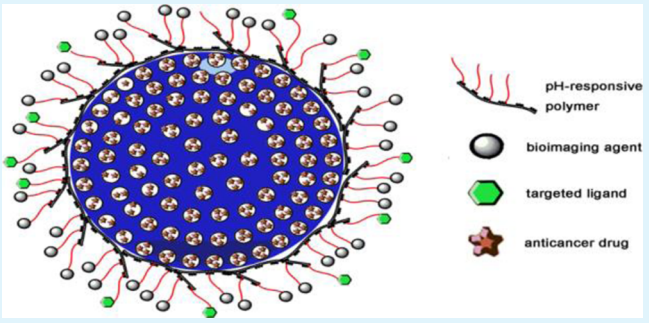

KEYWORDS: *hydroxylated mesoporous nanosilica, polyethylenimine, Gd-DTPA and folic acid, MR contrast agent, targeted drug delivery system*

1. INTRODUCTION

At present, plenty of anticancer drugs were developed and used for malignant tumor treatment. However, these drugs killed cancer cells, and also damaged normal cells at the same time leading to serious side effect on healthy tissue or organ.[1] Therefore, it was urgent to develop a drug delivery platform so as to reduce the damage to normal cells and relieve the pain of patient. Over the past decade, drug delivery system has sparked wide interest for its efficient cancer treatment, and the research on this field has made great progress.[2−4] Recently, nanomaterials and nanotechnology provided some new approaches to deliver anticancer drug to tumors and improved the clinical effects, attributing to the high drug delivery performance.[5−8]

Mesoporous nanosilica (MNS) was considered to be one of the most promising drug carriers because of its ordered pores, high surface area, and excellent biocompatibility.[9−13] However, unmodified MNS materials displayed low controlled release ability on anticancer drug to external triggers such as pH, enzyme, temperature, photo, and so on.[14−17] Therefore, it is demanded to develop some modification methods for MNS materials to improve the controlled release behavior. Currently, some organic matters with various functions were used to modify MNS to obtain different drug delivery nanoplatforms with high controlled release ability.[18]

Targeting delivery can increase the bioavailability of drugs to tumor tissues and reduce the toxicity on normal tissues. Folic acid (FA) has emerged as an attractive specific ligand for targeted anticancer drug delivery, because human cancer cells, such as HeLa cell, could usually overexpress folate receptors.[19−21] Previous reports indicated that nanoparticles (NPs) conjugated with folic acid displayed higher specificity and cellular internalization compared with NPs alone.[22−24] For

Received: February 5, 2015
Accepted: June 17, 2015
Published: June 17, 2015

DOI: 10.1021/acsami.5b04294
ACS Appl. Mater. Interfaces 2015, 7, 14192−14200

example, such NPs could be used as the targeted delivery therapeutic agents for cervix and breast cancers because the cells of those cancers possess rich folate receptors, and folic acid, through binding to the receptor, could act as "cancer cell locator" for targeted drug delivery and thus significantly facilitate the drug uptake of cancer cells.

For the clinical cancer patients, timely assessment of therapeutic response to a given therapy is also critical because that helps make the next treatment decisions. MR imaging has been well-established as a powerful tool for diagnosis and monitoring, because of its ability to noninvasively acquire 3D tomographic images with exquisite soft tissue contrast and anatomical detail.[25] Contrast agents such as gadolinium conjugated diethylenetriaminopentaacetic acid (Gd-DTPA) were used in these MR imaging procedures, which could help detect and display disease tissue. However, most clinically relevant Gd contrast agents are small, nontargeted compounds that will sometimes passively distribute into the interstitial space of tissues and organs, resulting in an insufficient signal enhancement. Hence, some nanoplatforms including dendrimers, polymers and silica nanoparticles which possessed a high payload of Gd ions were developed to compensate for the poor contrast signal.[21,26−29] Once coupled with an ability of targeted drug delivery, it is envisioned that those nanoplatforms can obtain a better clinical diagnosis and therapeutic effect.[30] Therefore, MR imaging-guided targeting chemotherapy has been a promising direction for improving the survival of cancer patients.[31] However, some issues still existed, especially good controlled release ability, and contrast enhancement could not be integrated effectively to the same delivery system.[32]

In this study, we reported a nanoplatform, hydroxylated MNS (HMNS) coated by branched polyethylenimine (PEI) coupled with Gd-DTPA and folic acid (Gd-FA-Si), as a targeted drug carrier and MR contrast agent. MNS was modified with 15% H_2O_2 solution to obtain more surface hydroxyl groups resulting in HMNS. Doxorubicin (DOX) was chosen as the anticancer drug and loaded into pores of HMNS. PEI was coated to HMNS through electrostatic attraction and hydrogen bond and acted as a pH-sensitive "gate" to control the release of drugs in HMNS because electrostatic interaction and hydrogen bond between PEI and HMNS could be easily affected by proton. In addition, PEI (positively charged) could, in some degree, facilitate the NPs to approach to cancer cells because those cells are usually negatively charged, and then slightly enhance the cellular uptake of the NPs.[33−35] Gd-DTPA and FA were linked to the PEI through the condensation reaction of the amide bond, which could make Gd-FA-Si possess high payload of Gd and good targeting for tumor cell. This Gd-FA-Si nanoplatform exhibited a high relaxivity per nanoparticle and facilitated cellular internalization. Therefore, this Gd-FA-Si nanoplatform loaded with drugs could maintain a sufficient drug concentration at the precise sites in the body and meanwhile be monitored under MR imaging, which will improve the therapeutic efficacy of patient.

2. EXPERIMENTAL SECTION

2.1. Materials. All chemical reagents were used as received without further purification. DEA, H_2O_2, dimethyl sulfoxide (DMSO), cetyltrimethylammonium bromine (CTAB) were purchased from Sinopharm Co. (Shanghai, China). DOX·HCl, PEI, $GdCl_3$, NHS, DCC and TEOS were received from Aladdin Co. (Shanghai, China). Diethylenetriaminopentaacetic acid (DTPA) dianhydride, Hoechst 33342, trypan blue, propidium iodide (PI) were purchased from Sigma-Aldrich. Co. (USA). Cell Counting Kit-8 (CCK-8) was obtained from Dojindo (Japan). Annexin V-FITC Apoptosis Detection Kit was purchased from BD Biosciences (San Jose, CA, USA). Other chemicals with analytical grade were obtained from Sinopharm Group Chemical Reagent Co., Ltd. (Shanghai, China).

2.2. Synthesis of HMNS. MNS was first synthesized as previously described.[17] Briefly, CTAB (2.0 g) was added into ethanol aqueous solution (10 mL/76 mL) under magnetic stirring at 80 °C. After 30 min, DEA (1 mL) was added into the transparent solution and then stirred continuously for 1 h. Then, TEOS (4 mL) was added into the resulting solution dropwise and stirred continuously for 12 h, and the MNS sample was achieved through centrifugation under 12000 rpm for 10 min. Subsequently, the MNS was dispersed in 15% H_2O_2 acid solution with pH 2.0 to remove the organic template and make more hydroxyl groups on the surface of MNS. Then, the solution was refluxed at 80 °C for 12 h, and this process was repeated for three times. Finally, the solution was centrifuged (12000 rpm for 10 min) and then dried at 60 °C for 12 h to obtain HMNS sample.

2.3. Preparation of DOX-Loaded Gd-FA-Si Nanoplatform. (1) 20 mg of HMNS was dispersed in 4 mL DOX·HCl solution (1 mg/mL) by shaking (200 rpm) at 25 °C for 12 h to obtain the sample of DOX-loaded HMNS (HMNS-DOX). And the drug storage capacity could be calculated by UV−vis spectrometer detecting variation of DOX·HCl before and after adding HMNS at a wavelength of 488 nm. (2) PEI (0.1 g) was added into the resulting HMNS-DOX solution of step 1 by stirring for 4 h. Subsequently, the obtained product, PEI-coated HMNS-DOX (PHMNS-DOX), was collected under 12 000 rpm for 10 min. (3) DTPA-dianhydride (30 mg) was reacted with NHS (30 mg) and DCC (100 μL) in distilled DMSO for 2 h at 60 °C. Then, PHMNS-DOX (20 mg) was added into the mixture solution and stirred overnight, and the solid particle sample was obtained and then collected through centrifugation. (4) $GdCl_3$ (25 mg) was dissolved in 10 mL of citrate buffer solution (pH 7.4). Subsequently, the solid particles of step 3 were dispersed into the $GdCl_3$ solution, and the DOX-loaded Gd -Si nanoplatform (Gd-Si-DOX) was finally obtained and then collected through centrifugation. (5) FA (10 mg) was reacted with NHS (10 mg) and DCC (20 μL) in distilled DMSO for 2 h at 60 °C. Then, Gd-Si-DOX was dispersed into the mixture solution and stirred overnight. DOX-loaded Gd-FA-Si nanoplatform was finally obtained and then collected through centrifugation.

2.4. Release Behavior Investigation of DOX. Gd-FA-Si-DOX was first placed at the bottom of a cuvette (10 mL), and then simulated body fluid (SBF) (3 mL) was slowly added (pH 7.4) into the cuvette to avoid disarranging the Gd-FA-Si-DOX particles. The pH of the supernatant was kept 7.4 during the initial 10 h, and adjusted to 5.5, 4.0, or 3.0 afterward through addition of HCl solution (0.05 M). To investigate the release performance, the concentration of DOX·HCl in the supernatant with time was determined using a UV−vis spectrophotometer (UV 2550, Shimadzu Co., Japan) at a wavelength of 488 nm. The cuvette was slightly shaken (20 rpm) throughout the release experiment.

2.5. MR Experiment. The capability of nanoplatform to influence the T_1 relaxation time was studied using a 9.4 T 8.9 cm wide bore, actively screened, vertical bore MR spectrometer (Bruker Biospoin GmbH, Germany). The longitudinal relaxation (T_1) rates were measured using the inversion recovery method. The T_1 relaxivity (r_1) was determined by a linear fit of the inverse relaxation times as a function of Gd concentration, which was determined using inductively coupled plasma mass spectrometry (ICP-MS) (ICP6300, Thermo Fisher Scientific Co., USA).

2.6. Leakage Investigation of Gd Ions from Gd-FA-Si Nanoplatform. Gd-FA-Si-DOX (10 mg) was dispersed into SBF (pH 7.4, 10 mL) by shaking for 50 h. After that, the colorless supernatant was obtained by centrifugation at 12 000 rpm/min. Then, Gd amount in the supernatant was measured by ICP-MS.

2.7. Cell Culture. HeLa and MDA-MB-231 cell lines, provided by the Institute of Biochemistry and Cell Biology of Chinese Academy of Sciences, were cultured in DMEM/high glucose medium containing 10% fetal bovine serum, 100 U/mL penicillin G sodium and 100 μg/mL streptomycin sulfate at 37 °C and 5% CO_2 in a humidified

DOI: 10.1021/acsami.5b04294
ACS Appl. Mater. Interfaces 2015, 7, 14192−14200

incubator. Cells were routinely harvested by treatment with a trypsin-ethylenediaminetetraacetic acid (EDTA) solution (0.25%).

2.8. In Vitro MR Imaging. HeLa cells were cultured in Dulbecco's modified eagle medium (DMEM)/high-glucose medium (Hyclone, China) supplemented with 10% (v/v) heat-inactivated fetal bovine serum and 1% penicillin-streptomycin at 37 °C in a humidified atmosphere with 5% CO_2. Prior to the treatment, HeLa cells were adjusted to a density of 5×10^5 cells/dish (60 mm diameter). Then cells were incubated using 0, 5, 20, and 40 μg/mL of Gd-FA-Si nanoplatforms. After a treatment for 1 h, media were removed, then cells were harvested, suspended, and fixed in 1.2 mL of PBS: 2% paraformaldehyde (1:1, v/v) at 4 °C for 1 h. Cells were centrifuged to remove paraformaldehyde at 800 rpm for 2 min, washed twice with PBS, resuspended in 50 μL PBS, and finally 150 μL of 0.8% agarose solutions were added onto cells. The mixture was carefully transferred into 5 mm NMR tube. Cells treated with four concentrations of Gd-FA-Si (0, 5, 20, and 40 μg/mL) were chosen and then observed under a 9.4 T MR spectrometer at room temperature.

2.9. FITC Accumulation Assay. HeLa and MDA-MB-231 seeded in 6-well plates (2×10^5 cells/well) were treated with FITC−Gd-Si (5 μg/mL) and FITC-Gd-FA-Si (5 μg/mL) for 1, 2, and 4 h at 37 °C. Aftrwards, the extracellular fluorescence was quenched with 0.4% trypan blue for 2 min, and cells were then trypsinized, washed three times with ice-cold pH 7.4 phosphate buffer solution (PBS), resuspended in 500 μL PBS, and measured by flow cytometry (BD FACScan flow cytometer, BD Biosciences). The fluorescent intensity was calculated by CellQuest software, and blanked by untreated cells.

2.10. Confocal Laser Scanning Microscope (CLSM) Observation. HeLa and MDA-MB-231 were seeded on 10 mm^2 glass coverslips placed in 24-well plates (5×10^4 cells/well) and cultured with DOX, Gd-FA-Si-DOX for 1, 2, and 4 h, followed by staining with Hoechst 33342 for additional 0.5 h at 37 °C in dark. Cells were washed twice with PBS and fixed with 4% paraformaldehyde for 30 min. Then, cells were mounted on glass slides and visualized using a confocal microscope (Zeiss LSM710 NLO, Germany).

2.11. In Vitro Cytotoxicity. Cytotoxicity was assessed by the standard CCK-8 assay. HeLa and MDA-MB-231 cells were seeded in 96-well plates (1×10^4 cells/well) and incubated with Gd-FA-Si, DOX·HCl, Gd-Si-DOX, and Gd-FA-Si-DOX of different concentrations for 24 h. After incubation with various samples, the culture medium was discarded, and cells were washed with PBS and then incubated in fresh medium containing 200 μL of 10% CCK-8 at 37 °C for 2h. The number of viable cells was measured at a wavelength of 450 nm with a Fluostar Optima microplate reader (BMG Labtechnologies, Germany). Measurements were made in eight independent experiments (n = 6, n indicates the number of wells in a plate for each experimental condition).

2.12. Cell Apoptosis and Cell Cycle Assay. HeLa and MDA-MB-231 cells were seeded in 60 mm plates (3×10^5 cells/well) and treated with Gd-FA-Si, DOX, Gd-Si-DOX, Gd-FA-Si-DOX, and Gd-FA-Si -DOX in the presence of excessive free folic acid for 24 h. For quantitative measurement of apoptosis, treated cells were harvested, washed twice with ice-cold PBS, stained with Annexin V-FITC, and PI for 15 min at room temperature in the dark, and then analyzed by a FACSCalibur system. For cell cycle assay, treated cells were collected by trypsinization (0.25% trypsin with EDTA). Then, cells were centrifuged and fixed with 70% ethanol at 0 °C overnight, washed twice in PBS, and resuspended in 200 mL of PBS containing 0.25 mg/mL RNase A for 30 min, and stained with 50 μL of PI (0.2 mg/mL in PBS) solution. After incubation in the dark at 4 °C for 30 min, the fluorescence of 10000 cells was analyzed by a FACSCalibur system.

2.13. Characterization. The morphologies of samples were observed on a scanning electron microscope (SEM) (Sirion 200, FEI Co., America). The structure and interaction were analyzed using a Fourier transform infrared (FTIR) spectrometer (Nicolet Co., America). Zeta potential of sample in distilled water was determined by zetasizer 3000 (Malvern, UK) at ambient temperature. Particle size distribution measurements were conducted on a dynamic light scattering (DLS) detector (Malvern, UK). Thermogravimetry analysis (TGA) and differential thermal analysis (DTA) of sample were performed using a thermogravimetry analyzer (Pyris 1, PerkinElmer Co., America).

3. RESULTS AND DISCUSSION

As shown schematically in Figure 1, the paramagnetic DOX loaded Gd-FA-Si (Gd-FA-Si-DOX) was developed as a tumor-targeted T_1 MR imaging contrast agent and drug delivery system by loading DOX into the pores of HMNS, which was then coated by PEI coupled with Gd-DTPA and folic acid. Therein, *N*-hydroxysuccinimide (NHS) and dicyclohexylcarbodiimide (DCC) were used to promote the condensation reaction between PEI and FA.

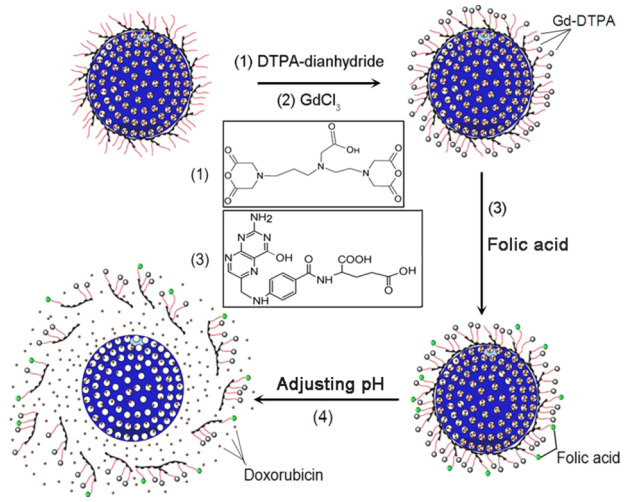

Figure 1. Schematic representation of paramagnetic targeted nanoplatform (Gd-FA-Si-DOX). Nanoparticles were fabricated through HMNS-DOX coated with PEI. Step 1 and 2: paramagnetic Gd^{3+} ions were conjugated to nanoparticle by DTPA; step 3: the resulting paramagnetic nanoparticles were further functionalized with folic acid, a tumor-targeting ligand; step 4: controlled release of DOX from nanoplatform through adjusting pH condition.

First of all, MNS with uniform particle size of about 105 nm (Figure 2a, b) was obtained through diethanolamine (DEA)-controlled hydrolysis of tetraethyl orthosilicate (TEOS). After that, the organic template in the pores of MNS was removed to obtain ordered pore structure through a refluxing in ethanol acid solution (Figure 2b). MNS was then modified using H_2O_2

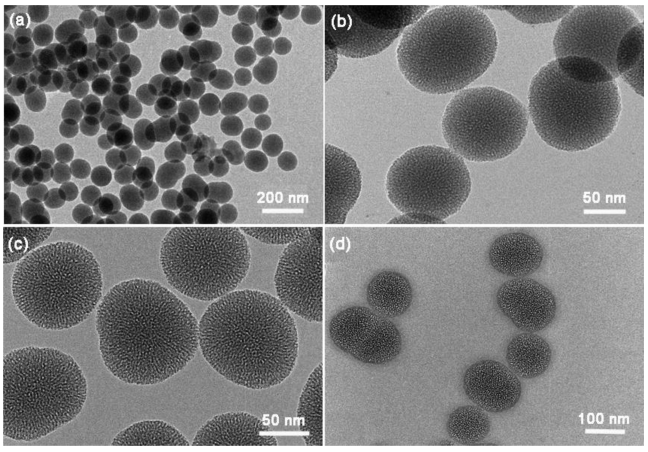

Figure 2. TEM images of (a, c) HMNS, (b) MNS, and (d) PHMNS.

DOI: 10.1021/acsami.5b04294
ACS Appl. Mater. Interfaces 2015, 7, 14192−14200

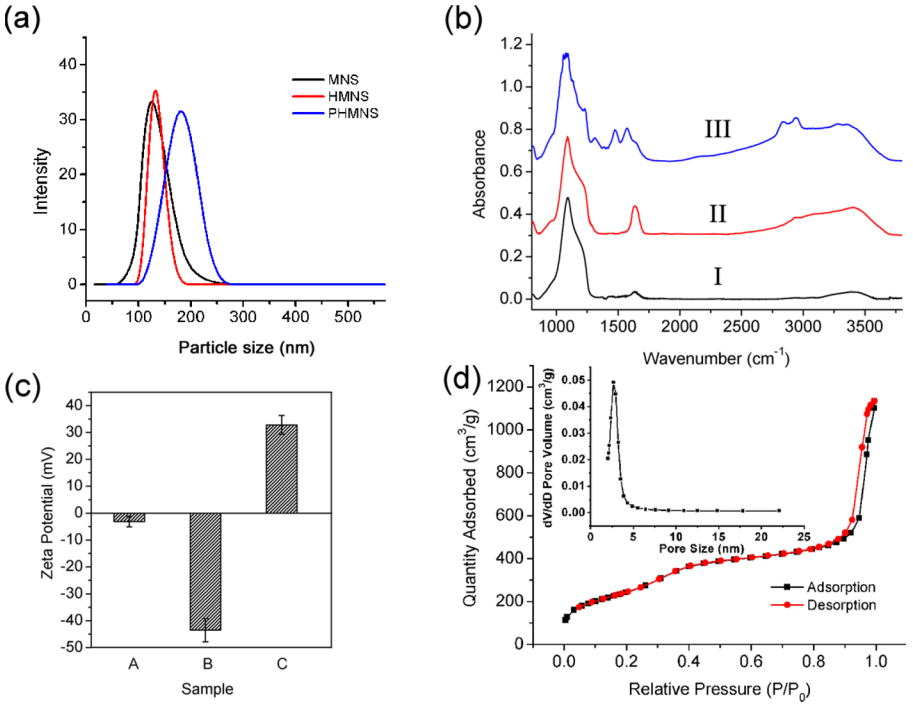

Figure 3. (a) Particle size distribution of HMNS, MNS, and PHMNS; (b) FT-IR spectra of MNS (I), HMNS (II), and PHMNS (III); (c) zeta potentials of MNS (sample A), HMNS (sample B), and PHMNS (sample C); (d) N_2 adsorption−desorption isotherms of HMNS (inset: pore size distribution of HMNS).

solution to obtain HMNS. From TEM image in Figure 2c, HMNS showed more obvious porosity, compared with MNS, indicating that HMNS can be a good carrier to storage drug molecules. To obtain pH-responsive property in nanoplatform, we coated a polymer layer consisting of PEI on the surface of HMNS through electrostatic interaction. As shown in Figure 2d, the PHMNS nanocomposite with a size of ∼150 nm possessed a well-defined core−shell structure and can be stably dispersed in pH 7.4 phosphate buffer solution (PBS).

Dynamic light scattering (DLS) experiments were performed to measure the particle sizes of the MNS, HMNS and PHMNS in PBS (Figure 3a). The narrow peaks of particle size distribution indicated that these nanoparticles possessed uniform shapes and good dispersion in the solution. It was found that the particle size of HMNS was slightly larger than MNS, indicating that hydrogen bonding interaction among particles increased because of plenty of hydroxyl groups on the surface of HMNS. Additionally, the particle size of PHMNS was larger than HMNS because of HMNS coated by PEI. Compared with the regular MNS (Figure 3bI), HMNS possessed a stronger peak at 1647 cm^{-1}, indicating plenty of silanol groups on the surface of HMNS. The peaks at 1635 and 3415 cm^{-1} in Figure 3bIII were assigned to —C−N and —N−H stretching vibrations, indicating that PEI successfully encapsulated HMNS. Zeta potential results illustrated that HMNS possessed more negative charges than MNS because of the increase of silanol groups on the surface (sample A and B in Figure 3c), so that HMNS could be easily coated with positive PEI (PHMNS) through electrostatic interaction. In addition, the protonation of PEI's amino groups in SBF made PHMNS positively charged (sample C in Figure 3c).

Figure 3d displayed the nitrogen adsorption−desorption isotherms and pore size distribution curve of HMNS. The isotherms exhibited that HMNS possessed ordered mesopores, high porosity and high specific surface area. The pore size distribution curve calculated by BJH method (inset of Figure 3d) illustrated a narrow pore size distribution (2−5 nm, dominantly 2.9 nm), which could help load plenty of anticancer drugs with suitable molecular size. DOX·HCl, a commonly used anticancer drug, was undoubtedly chosen as the model drug because the molecular size of DOX·HCl was estimated to be approximately 1.37 nm by Chemdraw software (see Figure S1 in the Supporting Information) and this enables DOX molecules well loaded in the pores of HMNS.

After loaded with DOX, HMNS was also equipped with PEI, Gd-DTPA, and FA to obtain a Gd-FA-Si-DOX drug delivery system, wherein PEI could act as the "gate" to control the release of DOX from the pores of HMNS. UV−vis analysis indicated that Gd-FA-Si possessed high drug storage capacity (242 μg/mg), which is helpful to provide continuous treatment for disease tissues when the drug is released. The release performances of Gd-FA-Si-DOX at different pH conditions were subsequently investigated (Figure 4a) and exhibited a pH-dependent behavior as shown in step 4 of Figure 1. At pH 7.4, the release amount of DOX could be negligible even within 10 h. However, when the pH was adjusted to 5.5, the release of DOX significantly increased, indicating that the electrostatic interaction between PEI and HMNS was broken because of the protonation effect. In addition, it could be seen that the release rate of DOX was much faster at pH 4.0 and pH 3.0. Subsequently, we investigated further the mechanism of DOX release from nanoplatform. It could be known that PEI was coated onto HMNS by electrostatic attraction and hydrogen bond interaction. Hydrogen bond between silanol groups of HMSN and amino groups of PEI chain could be easily destroyed by adjusting proton amount. Meanwhile, zeta potential of HMNS changed from −43 mV to −2.8 mV before and after loading DOX·HCl molecules because DOX·HCl was

DOI: 10.1021/acsami.5b04294
ACS Appl. Mater. Interfaces 2015, 7, 14192−14200

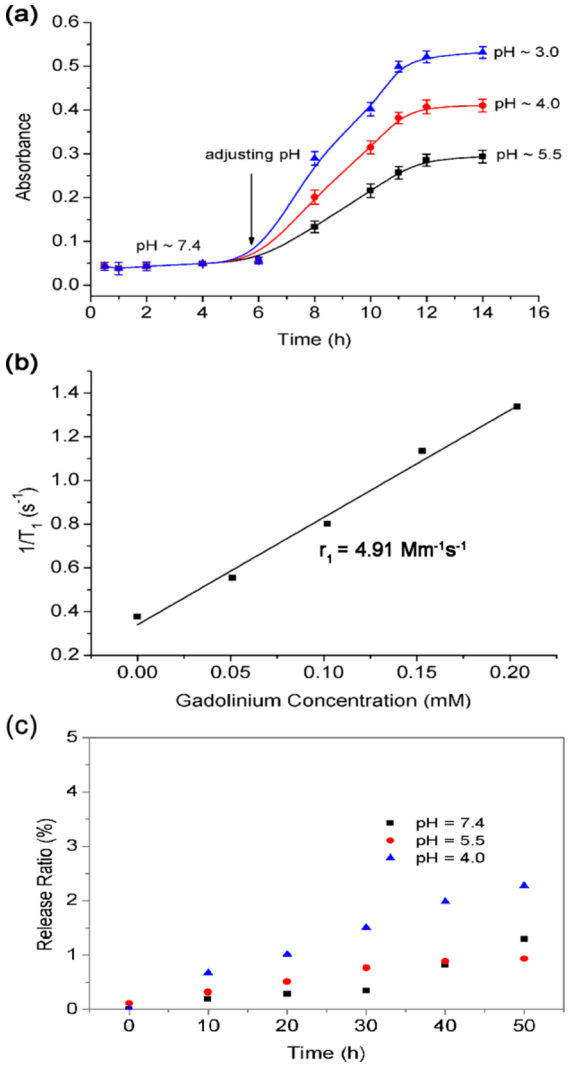

Figure 4. (a) Release behavior of DOX loaded in Gd-FA-Si nanoplatform under different pH conditions; (b) relaxivity (r_1) of Gd-FA-Si nanoplatform through the ratio of $1/T_1$ to Gd concentration (r_1 = 4.91 mM^{-1} s^{-1}); (c) release ratio of Gd ions from Gd-FA-Si nanoplatform under different pH conditions at 37 °C with time.

a weak base and positively charged (see Figure S2 in the Supporting Information). Moreover, isoelectric point of HMNS also changed from pH 3.0 to pH 6.3 before and after loading DOX·HCl molecules, which implied that HMNS-DOX changed to be positively charged upon below pH 6.3, and PEI chains coated onto HMNS-DOX would shed by electrostatic repulsion. Therefore, PEI chains would leave the nanoparticles faster with pH decrease, making DOX release faster. This pH-dependent behavior of Gd-FA-Si nanoplatform is valuable, because the microenvironments of extracellular tissues of tumors and their intracellular lysosomes and endosomes are usually acidic, and able to facilitate the drug release from Gd-FA-Si nanoplatform.

MR imaging is another key characteristic for Gd-FA-Si nanoplatform. FDA-approved Gd-DTPA was chosen as the MR contrast agent and linked to PHMNS, which could enhance the payload and the contrast effect. As previously reported,[36,37] Gd chelate was usually linked to the pores of nanoparticles to enhance contrast effect, while the narrow pores of the nanoparticles could lead to a slow water exchange rate which is detrimental to MR imaging effect. In this work, the Gd-FA-Si nanoplatform could avoid this issue because Gd chelate was linked on the surface of nanoparticle. In order to test the maximum amount of Gd-DTPA that PHMNS could load, TGA and DTA of PHMNS were performed as shown in Figure S3 (Supporting Information). Some water molecules of PHMNS were removed when temperature reached 129.2 °C as seen in TGA curve. With the increasing temperature, it could be seen from the DTA curve that PEI coating was decomposed through three steps, and the PEI mass ratio in PHMNS was 29.23%. The amino group amount of each PHMNS was then calculated up to 261000 (see Figure S4 in the Supporting Information). Therefore, each PHMNS was theoretically supposed to couple with 261000 Gd-DTPA. Actually, Gd ion amount of each nanoplatform (NP) was also measured by ICP-MS. The result indicated that each nanplatform possessed about 9.106×10^4, which is greater than one-third of theoretical value. The rest of amino groups of PEI can be probably used to form hydrogen bond with HMSN and bind to FA.

The relaxivity of Gd-FA-Si nanoplatform was then calculated through the ratio of proton relaxation ($1/T_1$) to Gd ion concentration (Figure 4b). Gd-FA-Si nanoplatform possessed an r_1 relaxivity value of 4.91 $mm^{-1}s^{-1}$ per Gd-DTPA, which was slightly higher than clinically used Gd.[38] Based on the results above, it is estimated that the theoretical and actual relaxivity of each nanoplatform is approximately up to 1.28×10^6 $mm^{-1}s^{-1}$ and 4.47×10^5 mm^{-1} s^{-1}, respectively. Compared with other Gd-conjugated MNS contrast agents,[27,39,40] the Gd-FA-Si nanoplatform exhibits better relaxivities. On the other hand, to ensure the safety of Gd-FA-Si nanoplatform as a contrast agent, the release amount of Gd ions from Gd-FA-Si was tested in PBS solutions under physiologically relevant pH conditions (pH 4.0, 5.5, and 7.0) at 37 °C (Figure 4c). The results suggested that the amount of the released Gd ions was rather low and could be negligible under those pH conditions, indicating that Gd-FA-Si possessed a good stability under physiologically relevant conditions.

The MR contrast enhancement of Gd-FA-Si on HeLa cells was further investigated. The MR images containing HeLa cells incubated with the nanoparticles with folic acid (Gd-FA-Si) and without folic acid (Gd−Si) are shown in Figure 5. It was found that Gd-FA-Si led rapidly to significant brightening of MR images compared with Gd−Si (Figure 5a), which indicated that folic acid could possess the targeting ability to HeLa cells and meanwhile make the contrast effect enhanced. In addition, HeLa cells incubated with Gd-FA-Si exhibited a significant MR signal intensity (T_1) decrease from 2680 to 742 ms (Figure 5b). Nevertheless, cells incubated with Gd−Si nanoparticle only showed a slight decrease in MR signal intensity from 2678 to 1451 ms, indicating that Gd-FA-Si nanoplatform could effectively bind to HeLa cells via the folate receptor and then enhance the contrast effect.

HeLa and MDA-MB-231 cells were used to evaluate the in vitro cytotoxicity of Gd-FA-Si, Gd-Si-DOX, and Gd-FA-Si-DOX through CCK-8 assay. The cells were incubated in the culture medium with Gd-FA-Si-DOX, Gd-Si-DOX, and Gd-FA-Si. As shown in Figure 6a, Gd-FA-Si with different concentrations did not result in an obvious decrease on the cell viability, indicating that the toxicity of Gd-FA-Si was low and negligible. As a positive control, HeLa and MDA-MB-231 cells incubated with free DOX, a hydrophilic anticancer drug, illustrated an obvious inhibitory effect. In addition, it could be seen from Figure 6c that free DOX in low concentration

DOI: 10.1021/acsami.5b04294
ACS Appl. Mater. Interfaces 2015, 7, 14192−14200

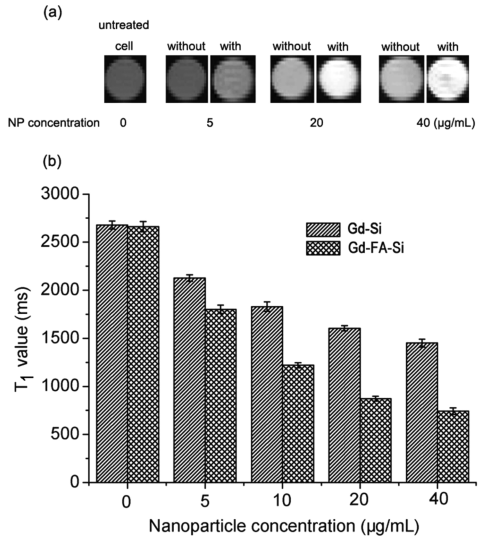

Figure 5. (a) T_1-weighted images (9.4 T) and (b) the corresponding T_1 values of the solutions of HeLa cells treated with different concentrations of nanoparticles with and without folic acid.

showed higher inhibitory effect for MDA-MB-231 cells, which implied that MDA-MB-231 cells were more sensitive to DOX. Compared with free DOX, Gd-Si-DOX had a slightly enhanced cytotoxicity on HeLa cells. While Gd-FA-Si-DOX showed a significantly enhanced cytotoxicity on HeLa cells, indicating that folic acid was beneficial for the uptake of Gd-FA-Si-DOX by HeLa cells and effect of DOX on the cancer cells (Figure 6b). Similar results were observed on MDA-MB-231 cells (Figure 6c), further confirming the potential application of the Gd-FA-Si-DOX as a drug delivery system.

CLSM was used to observe the Gd-FA-Si-DOX uptake of HeLa and MDA-MB-231 cells. In Figure 6d, the CLSM photographs of HeLa cells incubated with Gd-FA-Si-DOX for 1, 2, and 4 h displayed time-dependent fluorescence intensities. In the initial 1 h, weak fluorescence intensity was found in the cytoplasm, which indicated that just a few nanoplatforms were absorbed by HeLa cells. After incubation of 2 h, the fluorescence intensities of DOX in cellular nuclei increased, which presented that Gd-FA-Si-DOX had crossed the cell membrane and DOX molecules were released in the cytoplasm. With the increase in the incubation time, more and more DOX molecules were released in the cytoplasm. Additionally, few Gd-FA-Si-DOX nanoparticles were found on the outside of cells, which indicated that Gd-FA-Si-DOX possessed excellent targeting ability for HeLa cells. These results revealed the efficient intracellular delivery of DOX by the Gd-FA-Si nanoplatform. The similar results were obtained in the experiments using MDA-MB-231 cells (Figure 6e). However, for MDA-MB-231 cells, the fluorescence intensities of DOX were weak in cellular nuclei, indicating that cells were sensitive to DOX and had low drug-fastness.

Further, the apoptosis mechanisms of HeLa and MDA-MB-231 cells treated with Gd-FA-Si, free DOX, Gd-Si-DOX and Gd-FA-Si-DOX for 24 h were evaluated by flow cytometry (FCM) and fluorescence-activated cell sorting (FACS) protocols. Gd-FA-Si nanoparticles showed little influence on apoptosis of HeLa and MDA-MB-231 cells (Figure 7a, e). Additionally, free DOX could induce partially the late apoptosis of HeLa and MDA-MB-231 cells (Figure 7b, f). Compared with free DOX, Gd-Si-DOX would induce partially the late apoptosis and necrosis of HeLa and MDA-MB-231 cells, which could be associated with the cellular internalization of part of Gd-Si-DOX nanoparticles caused by endocytosis of cell membrane (Figure 7c, g). However, Gd-FA-Si-DOX remark-

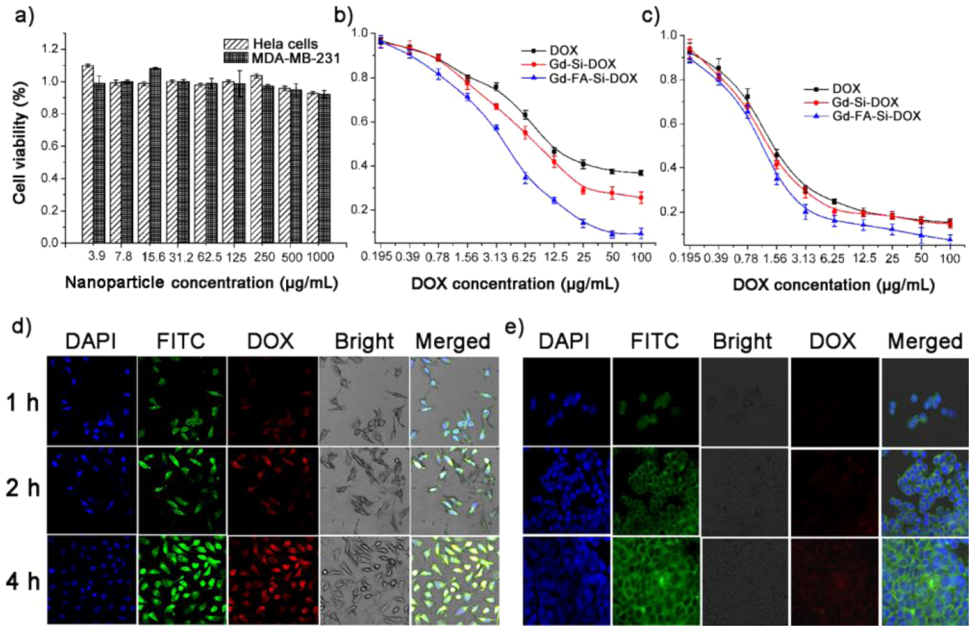

Figure 6. (a) CCK-8 assay for HeLa and MDA-MB-231 cells viabilities after incubation with different concentrations of Gd-FA-Si nanoplatform. Cells viabilities of (b) HeLa and (c) MDA-MB-231 treated with free DOX, Gd−Si-DOX, Gd-FA-Si-DOX at different concentrations for 12 h (concentrations of Gd-Si-DOX and Gd-FA-Si-DOX were represented by concentration of DOX same as free DOX). CLSM observations of FITC labeled Gd-FA-Si-DOX nanoplatform uptake of cells and DOX release in (d) HeLa and (e) MDA-MB-231 cells. For each panel, the images from left to right show cell nuclei stained by DAPI (blue; DAPI = 4′, 6-diamidino-2-phenylindole), FITC fluorescence in cells (green), DOX fluorescence in cells (red), bright field, and the merged one of the left four images. All images share the same scale bar.

DOI: 10.1021/acsami.5b04294
ACS Appl. Mater. Interfaces 2015, 7, 14192−14200

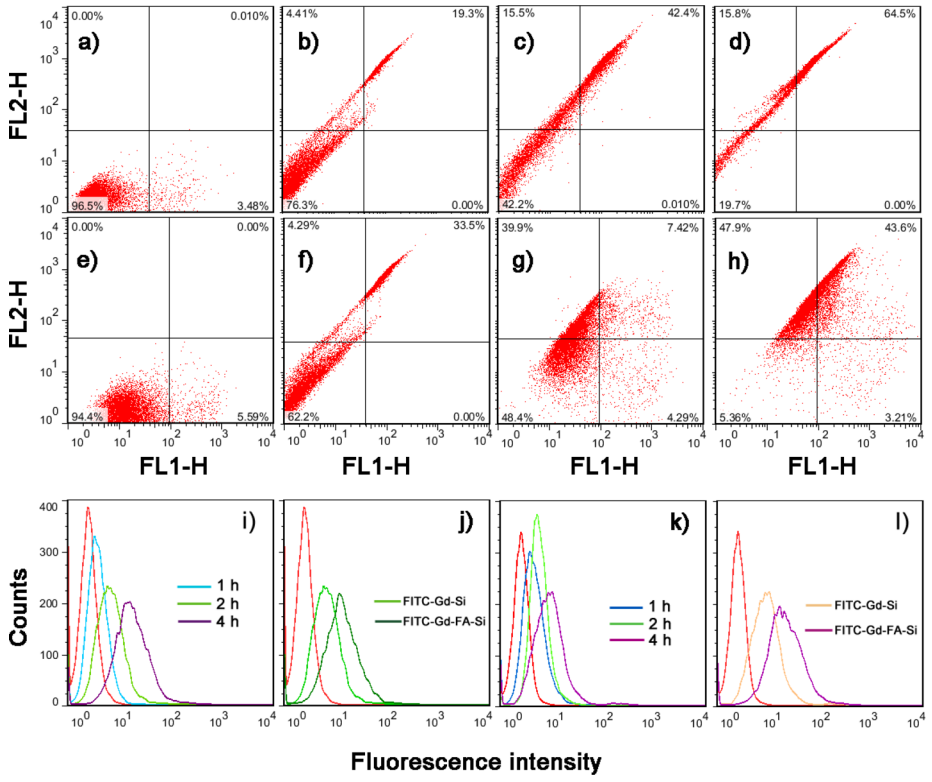

Figure 7. Flow cytometry analysis for apoptosis of (a–d) HeLa and (e–h) MDA-MB-231 cells induced by Gd-FA-Si, free DOX, Gd-Si-DOX, and Gd-FA-Si-DOX, respectively. Flow cytometry histograms show the FITC fluorescence intensity in (i, j) HeLa and (k, l) MDA-MB-231 cell nuclei separated from the whole cells. (i–l) Red lines represent the negative control samples. (i, k) Samples treated with FITC-labeled Gd-FA-Si nanoplatform for different times, and (j, l) samples treated with FITC-labeled Gd-Si and Gd-FA-Si, respectively, for 2 h.

ably accelerated the apoptosis and necrosis of HeLa and MDA-MB-231 cells at the same particle concentrations (Figure 7d, h), which implied that folic acid possessed good targeting and could increase cell uptake of nanoplatforms. Therefore, the Gd-FA-Si-DOX could induce HeLa and MDA-MB-231 cells apoptosis by a targeting apoptosis-accelerating effect between FA and DOX, which should be attributed to the continuously intracellular release of DOX from Gd-FA-Si-DOX nanoplatform, and a good targeting of FA toward HeLa and MDA-MB-231 cells. In addition, quantification with flow cytometric measurements of HeLa and MDA-MB-231 cells indicated that the amount of Gd-FA-Si-DOX was obviously greater than that of Gd-Si-DOX (Figure 7j, l). And with increasing time, the fluorescence intensities of HeLa and MDA-MB-231 cells were becoming higher (Figure 7i, k). More importantly, compared with Gd-Si-DOX, MR contrast enhancements of Gd-FA-Si-DOX were also successfully observed. These results showed that Gd-FA-Si-DOX could be a good therapeutic and imaging agent.

4. CONCLUSIONS

A new Gd-FA-Si-DOX nanoplatform was developed as a tumor-targeted drug delivery system and T_1 MR contrast agent. Anticancer drug (DOX) could be loaded into the pores of HMNS. Then, PHMNS, PEI coated on HMNS, were coupled with Gd-DTPA and FA to obtain high contrast enhancement and targeting. The release of DOX from this nanoplatform showed a pH-controlled property in acidic environments. Additionally, the outer PEI layer improved the biocompatibility and colloid stability of the Gd-FA-Si nanoplatform, and the CCK-8 assay showed a low cytotoxicity of the nanoplatform. The flow cytometry and CLSM observations revealed that the Gd-FA-Si-DOX could target cancer cells through FA receptors and release DOX in cytoplasm to kill cancer cells. Meanwhile, the excellent MR contrast enhancement of the nanoplatform on cells was obtained, indicating the potential application of the nanoplatform as T_1 contrast agents. Thus, the Gd-FA-Si-DOX nanoplatform could be a promising drug delivery system for the targeted and MR imaging-guided cancer treatment.

■ ASSOCIATED CONTENT

Ⓢ Supporting Information

Additional figures for DOX molecular size, TG analysis of PHMNS, and analysis of the amounts of amino groups on the surface of PHMNS. The Supporting Information is available free of charge on the ACS Publications website at DOI: 10.1021/acsami.5b04294.

■ AUTHOR INFORMATION

Corresponding Authors

*Tel: +86-551-65786021. E-mail: xinzhang@ahau.edu.cn.
*Tel: +86-551-65591413. E-mail: zywu@ipp.ac.cn.

Author Contributions

†G.Z. and J.G. are cofirst authors.

Notes

The authors declare no competing financial interest.

■ ACKNOWLEDGMENTS

The authors acknowledge financial support from the National Key Foundation for Exploring Scientific Instrument of China (2013YQ17058507), the National Natural Science Foundation

DOI: 10.1021/acsami.5b04294
ACS Appl. Mater. Interfaces 2015, 7, 14192–14200

of China (21072002, 21407151), the Key Program of the Chinese Academy of Sciences (KSZD-EW-Z-022-05), and the Scientific and Technological Project of Anhui Province of China (1206c0805014).

REFERENCES

(1) Nagasubramanian, R.; Innocent, F.; Ratain, M. Pharmacogenetics in Cancer Treatment. *Annu. Rev. Med.* **2003**, *54*, 437−452.
(2) Li, K. C.; Pandit, S. D.; Guccione, S.; Bednarski, M. D. Molecular Imaging Applications in Nanomedicine. *Biomed. Microdevices* **2004**, *6*, 113−116.
(3) Moghimi, S. M.; Hunter, A. C.; Murray, J. C. Nanomedicine: Current Status and Future Prospects. *FASEB J.* **2005**, *19*, 311−330.
(4) Nasongkla, N.; Bey, E.; Ren, J.; Ai, H.; Khemtong, C.; Guthi, J. S. Multifunctional Polymeric Micelles as Cancer-Targeted, MRI-Ultrasensitive Drug Delivery Systems. *Nano Lett.* **2006**, *6*, 2427−2430.
(5) Douglas, S. M.; Bachelet, I.; Church, G. M. A Logic-Gated Nanorobot for Targeted Transport of Molecular Payloads. *Science* **2012**, *335*, 831−834.
(6) Chou, L. T.; Zagorovsky, K.; Chan, W. C. W. DNA Assembly of Nanoparticle Superstructures for Controlled Biological Delivery and Elimination. *Nat. Nanotechnol.* **2014**, *9*, 148−155.
(7) Choi, H. S. Nanoparticle Assembly: Building Blocks for Tumor Delivery. *Nat. Nanotechnol.* **2014**, *9*, 93−94.
(8) Baeza, A.; Guisasola, E.; Ruiz, H. E.; Vallet, R. M. Magnetically Triggered Multidrug Release by Hybrid Mesoporous Silica Nanoparticles. *Chem. Mater.* **2012**, *24*, 517−524.
(9) Zhang, G. L.; Gao, J. L.; Qian, J. C.; Cai, D. Q.; Zheng, K.; Yu, Z. W.; Zhong, K.; Zhang, X.; Wu, Z. Y. A Multifunctional Magnetic Composite Material as a Drug Delivery System and a Magnetic Resonance Contrast Agent. *Part. Part. Syst. Charact.* **2014**, *31*, 976−984.
(10) He, Q. J.; Shi, J. L. Mesoporous Silica Nanoparticle Based Nano Drug Delivery Systems: Synthesis, Controlled Drug Release and Delivery, Pharmacokinetics and Biocompatibility. *J. Mater. Chem.* **2011**, *21*, 5845−5855.
(11) Özalp, V. C.; Pinto, A.; Nikulina, E.; Chuvilin, A.; Schäfer, T. Synthesis and Characterization of Fluorescent, Radio-Opaque, and Paramagnetic Silica Nanoparticles for Multimodal Bioimaging Application. *Part. Part. Syst. Charact.* **2014**, *31*, 161−167.
(12) Radhakrishnan, K.; Gupta, S.; Gnanadhas, D. P.; Ramamurthy, P. C.; Chakravortty, D.; Raichur, A. M. Protamine-Capped Mesoporous Silica Nanoparticles for Biologically Triggered Drug Release. *Part. Part. Syst. Charact.* **2014**, *31*, 449−458.
(13) Palanikumar, L.; Choi, E. S.; Cheon, J. Y.; Joo, S. H.; Ryu, J. H. Noncovalent Polymer-Gatekeeper in Mesoporous Silica Nanoparticles as a Targeted Drug Delivery Platform. *Adv. Funct. Mater.* **2015**, *25*, 957−965.
(14) Zou, Y.; Song, Y.; Yang, W.; Meng, F.; Liu, H.; Zhong, Z. Y. Galactose-Installed Photo-Crosslinked pH-Sensitive Degradable Micelles for Active Targeting Chemotherapy of Hepatocellular Carcinoma in Mice. *J. Controlled Release* **2014**, *193*, 154−161.
(15) Wu, L.; Zou, Y.; Deng, C.; Cheng, R.; Meng, F.; Zhong, Z. Y. Intracellular Release of Doxorubicin from Core-Crosslinked Polypeptide Micelles Triggered by Both pH and Reduction Conditions. *Biomaterials* **2013**, *34*, 5262−5272.
(16) Cheng, R.; Meng, F. H.; Deng, C.; Klok, H. A.; Zhong, Z. Y. Dual and Multi-Stimuli Responsive Polymeric Nanoparticles for Programmed Site-Specific Drug Delivery. *Biomaterials* **2013**, *34*, 3647−3657.
(17) Zhang, G. L.; Yang, M. L.; Cai, D. Q.; Zheng, K.; Zhang, X.; Wu, L. F.; Wu, Z. Y. Composite of Functional Mesoporous Silica and DNA: An Enzyme-Responsive Controlled Release Drug Carrier System. *ACS Appl. Mater. Interfaces* **2014**, *6*, 8042−8047.
(18) Du, L.; Liao, S. J.; Khatib, H. A.; Stoddart, J. F.; Zink, J. I. Controlled-Access Hollow Mechanized Silica Nanocontainers. *J. Am. Chem. Soc.* **2009**, *131*, 15136−15142.
(19) Sudimack, J.; Lee, R. J. Targeted Drug Delivery via the Folate Receptor. *Adv. Drug Delivery Rev.* **2000**, *41*, 147−162.
(20) Low, P. S.; Henne, W. A.; Doorneweerd, D. D. Discovery and Development of Folic-Acid-Based Receptor Targeting for Imaging and Therapy of Cancer and Inflammatory Diseases. *Acc. Chem. Res.* **2008**, *41*, 120−129.
(21) Lu, Y.; Low, P. S. Folate-Mediated Delivery of Macromolecular Anticancer Therapeutic Agents. *Adv. Drug Delivery Rev.* **2002**, *54*, 675−693.
(22) Cheng, Z. L.; Thorek, D. J.; Tsourkas, A. Gadolinium-Conjugated Dendrimer Nanoclusters as a Tumor-Targeted T_1 Magnetic Resonance Imaging Contrast Agent. *Angew. Chem., Int. Ed.* **2010**, *49*, 346−350.
(23) Zhu, Y.; Fang, Y.; Kaskel, S. Folate-Conjugated Fe_3O_4@SiO_2 Hollow Mesoporous Spheres for Targeted Anticancer Drug Delivery. *J. Phys. Chem. C* **2010**, *114*, 16382−16388.
(24) Chan, M. H.; Lin, H. M. Preparation and Identification of Multifunctional Mesoporous Silica Nanoparticles for in Vitro and in Vivo Dual-Mode Imaging, Theranostics, and Targeted Tracking. *Biomaterials* **2015**, *46*, 149−158.
(25) Cheng, Z. L.; Thorek, D. J.; Tsourkas, A. Porous Polymersomes with Encapsulated Gd-Labeled Dendrimers as Highly Efficient MRI Contrast Agents. *Adv. Funct. Mater.* **2009**, *19*, 3753−3759.
(26) Duarte, M. G.; Gil, M. H.; Peters, J. A.; Colet, J. M.; Elst, L. V.; Muller, R. N. Synthesis, Characterization, and Relaxivity of Two Linear Gd(DTPA)−Polymer Conjugates. *Bioconjugate Chem.* **2001**, *12*, 170−177.
(27) Rieter, W. J.; Kim, J. S.; Taylor, K. M. L.; An, H.; Lin, W.; Tarrant, T. Hybrid Silica Nanoparticles for Multimodal Imaging. *Angew. Chem. Int. Ed.* **2007**, *46*, 3680−3682.
(28) Zhang, D.; Gao, A.; Xu, Y.; Yin, X. B.; He, X. W.; Zhang, Y. K. Gd-Al Co-Doped Mesoporous Silica Nanoparticles Loaded with $Ru(bpy)_3^{2+}$ as a Dual-Modality Probe for Fluorescence and Magnetic Resonance Imaging. *Analyst* **2014**, *139*, 4613−4619.
(29) Lee, G. Y.; Qian, W. P.; Wang, L. Y.; Wang, Y. A.; Staley, C. A.; Satpathy, M. Theranostic Nanoparticles with Controlled Release of Gemcitabine for Targeted Therapy and MRI of Pancreatic Cancer. *ACS Nano* **2013**, *3*, 2078−2089.
(30) Wang, C.; Cheng, L.; Liu, Z. Drug Delivery with Upconversion Nanoparticles for Multifunctional Targeted Cancer Cell Imaging and Therapy. *Biomaterials* **2011**, *32*, 1110−1120.
(31) Liang, C.; Diao, S.; Wang, C.; Gong, H.; Liu, T.; Liu, Z. Tumor Metastasis Inhibition by Imaging-Guided Photothermal Therapy with Single-Walled Carbon Nanotubes. *Adv. Mater.* **2014**, *26*, 5646−5652.
(32) Xia, T.; Kovochich, M.; Liong, M.; Meng, H.; Kabehie, S.; George, S. Polyethyleneimine Coating Enhances the Cellular Uptake of Mesoporous Silica Nanoparticles and Allows Safe Delivery of siRNA and DNA Constructs. *ACS Nano* **2009**, *3*, 3273−3286.
(33) Liu, M.; Zhang, X.; Yang, B.; Li, Z.; Deng, F.; Yang, Y.; Zhang, X.; Wei, Y. Fluorescent Nanoparticles from Starch: Facile Preparation, Tunable Luminescence and Bioimaging. *Carbohydr. Polym.* **2015**, *121*, 49−55.
(34) Rosenholm, J. M.; Meinander, A.; Peuhu, E.; Niemi, R.; Eriksson, J. E.; Sahlgren, C.; Linden, M. Targeting of Porous Hybrid Silica Nanoparticles to Cancer Cells. *ACS Nano* **2009**, *3*, 197−206.
(35) Rosenholm, J. M.; Sahlgren, C.; Linden, M. Towards Multifunctional, Targeted Drug Delivery Systems Using Mesoporous Silica Nanoparticles−Opportunities & Challenges. *Nanoscale* **2010**, *2*, 1870−1883.
(36) Steinbacher, J. L.; Lathrop, S. A.; Cheng, K.; Hillegass, J. M.; Kauppinen, R. A.; Mossman, B. T. Gd-Labeled Microparticles in MRI: in Vivo Imaging of Microparticles After Intraperitoneal Injection. *Small* **2010**, *6*, 2678−2682.
(37) Duncan, A. K.; Klemm, P. J.; Raymond, K. N.; Landry, C. C. Silica Microparticles as a Solid Support for Gadolinium Phosphonate Magnetic Resonance Imaging Contrast Agents. *J. Am. Chem. Soc.* **2012**, *134*, 8046−8049.
(38) Gupta, A.; Campo, L.; Rehmanjan, B.; Willis, S. A.; Waddington, L. J.; Gardner, T. S.; Kirby, N.; Price, W. S.; Moghaddam, M. J.

DOI: 10.1021/acsami.5b04294
ACS Appl. Mater. Interfaces 2015, 7, 14192−14200

Evaluation of Gd-DTPA-Monophytanyl and Phytantriol Nanoassemblies as Potential MRI Contrast Agents. *Langmuir* **2015**, *31*, 1556−1563.
(39) Santra, S.; Bagwe, R. P.; Dutta, D.; Stanley, J. T.; Walter, G. A.; Tan, W. Synthesis and Characterization of Fluorescent, Radio-Opaque, and Paramagnetic Silica Nanoparticles for Multimodal Bioimaging Applications. *Adv. Mater.* **2005**, *17*, 2165−2169.
(40) Taylor, K. M. L.; Kim, J. S.; Rieter, W. J.; An, H.; Lin, W. Mesoporous Silica Nanospheres as Highly Efficient MRI Contrast Agents. *J. Am. Chem. Soc.* **2008**, *130*, 2154−2155.

DOI: 10.1021/acsami.5b04294
ACS Appl. Mater. Interfaces 2015, 7, 14192−14200